

Photoelectrochemical and Spectroscopic Studies of Colloidal Nano-Particles of Mixed TiO₂/V₂O₅ Metal-Oxide Semiconductors

Kasem K. Kasem^{1*}, Aubrey Finley¹, James Folberth², Maarij Syed², Elaine Kirkpatrick²

¹Department of Science, Mathematics, and Informatics, School of Art and Science, Indiana University Kokomo, Kokomo, USA;

²Rose Hulman Institute of Technology, Terre Haute, USA.

Email: *kkasem@iuk.edu

Received February 3rd, 2012; revised March 9th, 2012; accepted April 15th, 2012

ABSTRACT

Due to its importance in hydrogen production during the photolysis process of aqueous suspensions process, mixed TiO₂/V₂O₅ metal-oxide semiconductors were prepared and subjected to crystal structure investigation using X-ray technique. The photoelectrochemical behavior of these TiO₂/V₂O₅ was investigated by photolysis of aqueous suspensions of these oxides containing [Fe(CN)₆]⁴⁻. X-ray diffraction analysis indicated that the TiO₂ crystallites grow in the (1 0 1) direction, while The V₂O₅ crystallites seem to be growing in the (4 2 0) direction, with increasing concentration of V₂O₅. Photolysis studies show that photochemical activities that maintained the [Fe(CN)₆]⁴⁻/[Fe(CN)₆]³⁻ redox reversibility increased by increasing V₂O₅ up to 50% and then decreased at greater percentages. Aqueous nano systems used in these studies retained their stability as indicated by the reproducibility of their photo-catalytic activities.

Keywords: TiO₂/V₂O₅; Nanoparticles; Semiconductors; Photolysis; Hydrogen Production

1. Introduction

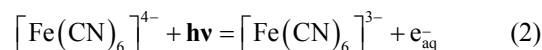
Water as an abundant source of hydrogen has been a focus of interest of green energy researchers. Photo-dissociation of water into hydrogen and oxygen using powder suspensions of some semiconductors was recently reported by several researchers [1-8]. Most of the studies on the photo-dissociation of water were done over compact semiconductor electrodes. Colloidal semiconductors were used because of their larger surface area and their ability to carry out all reactions that were previously associated with massive semiconductor electrodes. In some systems, platinized semiconductors powders such as TiO₂ were used for simultaneous production of oxygen and hydrogen. Several methods were used to generate ordered assemblies of narrow band gap semiconductor nanostructures for harvesting visible-light energy. In most of these methods, one material with a specific band gap is being produced. Some studies, performed on metal chalcogenides such as sulfides, selenides, tellurides [9-16], reported low conversion efficiencies. The photocurrent obtained using such nano-particle assemblies is often low because fast charge recombination limits photocurrent and consequently hydrogen generation.

Hydrated electrons (e_{aq}^-) can play an important role in

the photodissociation of water through this reaction:



This reaction proceeds with a rate $k \approx 1 \times 10^{10} M^{-1} \cdot sec^{-1}$ [17]. The molecular orbital structure of hexacyanoiron(II) or [Fe(CN)₆]⁴⁻ allows electronic transition under the photo excitation condition and the reaction produces hydrated electrons according to the following equation:



The oxidation process compromises the reported high rate. The disadvantage of a homogeneous process for hydrogen production is its irreversibility. However, this disadvantage can be overcome through the use of a semiconductor system which acts as an electron donor and reduces [Fe(CN)₆]³⁻ back to [Fe(CN)₆]⁴⁻. Achieving such a goal will create the conditions of reversible ergodynamics. The conditions could be reached if the rate of reduction of [Fe(CN)₆]³⁻ could be equated to the rate of formation of hydrated electrons from [Fe(CN)₆]⁴⁻.

p-Type semiconductors particles can be used for the heterogeneous reduction of hydrogen ions to generate hydrogen if a suitable hole-scavenger is present in the suspension media. With the high rate of photo-generation of hydrated electrons in homogenous solutions, it is pos-

*Corresponding author.

sible that hydrogen can be generated heterogeneously and homogeneously by the photolysis of colloidal particles suspended in Ferro-cyanide solutions at room temperature.

In this paper, we highlight the preparation of TiO₂/V₂O₅ and the effects that the percentage of V₂O₅ may cause on the growth and orientation of each oxide in their common crystal structure and on the rate of hydrogen production during the photolysis process using visible light photons. The possibility of using these systems in a solar energy-based photolysis cell that achieve the goal of reversible, cyclic, and efficient process for hydrogen production is explored.

2. Experimental

2.1. Reagents

All reagents were of analytical grade. Titanium Oxide TiO₂ doped with V₂O₅ was prepared as described elsewhere [18] using NaVO₃ and TiCl₃ as starting materials.

2.2. Instrumentation

A BAS 100W electrochemical analyzer (Bioanalytical Co.) was used to perform the electrochemical studies. Steady state reflectance spectroscopy was performed using a Shimadzu UV-2101 PC. An Olympus BX-FLA60 reflected light.

2.3. X-Ray Studies

X-ray diffraction studies were carried out on a Bruker AXS D8 Focus X-ray diffraction machine. The basic principle of operation relies on Bragg diffraction. The setup utilizes X-rays from a copper target that have their main intensity at 154.2 pm. This average wavelength actually has two contributions; the dominant contribution is from Copper K_{α1} (λ = 154.06 pm) and a secondary contribution from Copper K_{α2} (λ = 154.44 pm). Bragg diffraction is modeled by the following expression:

$$n\lambda = 2d \sin \theta \quad (3)$$

Here n is the diffraction order ($n = 1$ for our analysis), λ is the x-ray wavelength, d is the distance between scattering planes, and θ is the angle of diffraction. The diffraction data are in the form of intensities versus scattering angles. Strong peaks correspond to constructive interference between certain scattering planes, and allow for the evaluation of the distance between the scattering planes and their orientation. The scattering angle (2θ) was varied from 10° to 90° with a resolution of 0.02°. The resulting signal was integrated long enough to provide clear unambiguous peaks. Once the peaks are identified as resulting from a certain constituent (TiO₂ or

V₂O₅), they are fitted to a Gaussian curve with the help of mathematical analysis software such as Maple. This curve fitting yields the full width at half maximum (FWHM) which is then used to find the Diffracting Crystallite Size (DCS), t , (in angstroms) with the help of the following expression [19].

$$t = \frac{0.9\lambda}{FWHM \cdot \cos(2\theta)} [\text{Å}] \quad (4)$$

This in turn can reveal information about growth trends of certain crystallites (orientations) with increasing concentration of various constituents.

2.4. Photolysis Cell

The electrolysis cell was 100 mL one compartment a Pyrex cell with a quartz window facing the irradiation source. The working electrode was a 10-cm² platinum gauze cylinder with a fixed potential of 0.100 Volt more negative than the reduction potential of [Fe(CN)₆]³⁻. Suspensions were stirred with a magnetic stirrer during the measurements. An Ag/AgCl/Cl⁻ reference electrode was also fitted in this compartment. A platinum counter-electrode was housed in a glass cylinder sealed in one end with a fine porosity glass frit. Unless otherwise stated, the photolysis took place in 0.2 M phosphate pH 6 buffer, containing 0.02 M K₄[Fe(CN)₆]. The cell diagram and the bases for our choice of this solution is mentioned in our previous work [4,7].

Irradiations were performed with a solar simulator 300 watt xenon lamp (Newport) with an IR filter. The measured photo current was normalized considering two photons per one hydrogen molecule.

3. Results and Discussions

3.1. Crystallographic Growth of TiO₂/V₂O₅ Mixtures

X-ray spectrum studies were performed on TiO₂ mixed with 10%, 30%, 50%, 90% V₂O₅. Samples of these spectra are shown in **Figure 1**. These spectra indicate that there are 4 strong peaks corresponding to constructive interference between certain scattering planes, and allow for the evaluation of the distance between the scattering planes and their orientation. Analysis of these strong peaks corresponding to $2\theta = 25.3, 15, 61, \text{ and } 63$ the following procedure was adopted to calculate DCS (Diffracting Crystallite Size).

- Used XRD plots to locate peaks.
- Fitted a Gaussian curve to each peak using Maple.
- Analyzed curve to calculate FWHM.
- Found the Diffracting Crystallite Size t using equation 4, where $\lambda = 1.540598 \text{ Å} [\text{Cu-K}\alpha_1]$.

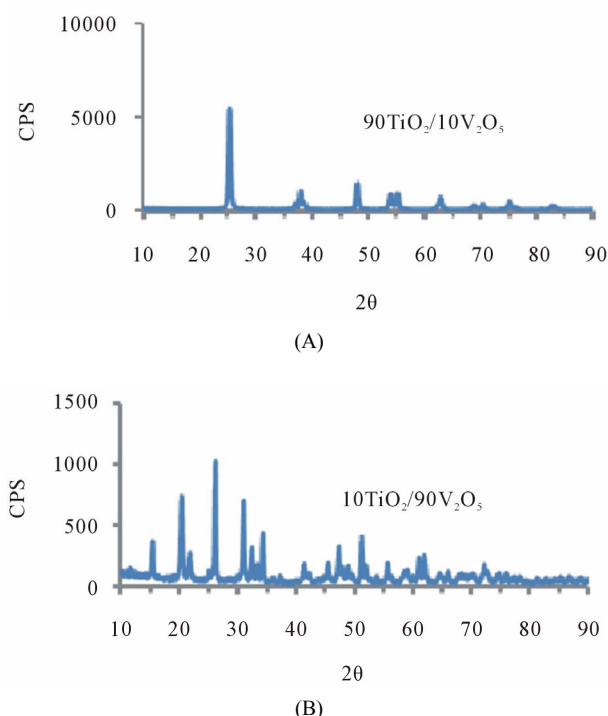


Figure 1. X-ray patterns of TiO₂/V₂O₅ mixtures as titled.

The results displayed in **Figure 2** particularly indicate that:

1) For $2\theta = 25$ TiO₂ peak The TiO₂ crystallites seem to be growing in the (1 0 1) direction, with increasing concentration of V₂O₅.

2) For $2\theta = 15$ V₂O₅ peak The V₂O₅ crystallites seem to be shrinking in the (2 0 0) direction, with increasing concentration of V₂O₅.

3) For $2\theta = 61$ V₂O₅ peak The V₂O₅ crystallites seem to be growing in the (4 2 0) direction, with increasing concentration of V₂O₅.

4) For $2\theta = 63$ TiO₂ peak The TiO₂ crystallites seem to be growing in the (2 0 4) direction, with increasing concentration of V₂O₅.

The studies generally indicated that:

1) TiO₂ DCS grows in multiple orientations with increasing V₂O₅ concentration.

2) V₂O₅ DCS grows in certain orientations and shrinks in other orientations with increasing V₂O₅ concentration.

3.2. Band-Energy Map of the Studied Oxides

Steady state reflectance spectra of the colloidal nanoparticles of TiO₂/V₂O₅ mixtures are shown in **Figure 3(A)**. The approximate values of the band gaps derived from this figure are listed in **Table 1**. However, the following Equations were used to determine whether direct or indirect transition band structures exist in these doped oxides [20]:

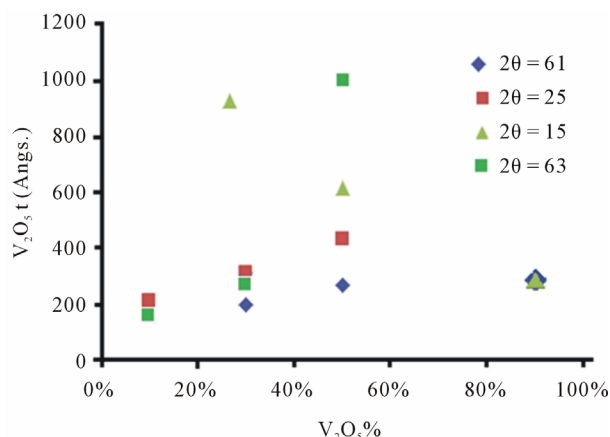


Figure 2. Plot of Equation 4 for the studied oxides at different 2θ .

$$(\alpha E_{\gamma})^2 \propto E_{\gamma} - E_{gd} \quad (5)$$

$$\alpha \propto \frac{(E_{\gamma} + E_p - E_{gi})^2}{e^{(E_{\gamma}/kT)} - 1} + \frac{(E_{\gamma} - E_p - E_{gi})^2 e^{(E_{\gamma}/kT)}}{e^{(E_{\gamma}/kT)} - 1} \quad (6)$$

where α is absorption coefficient, E_g is the optical band gap.

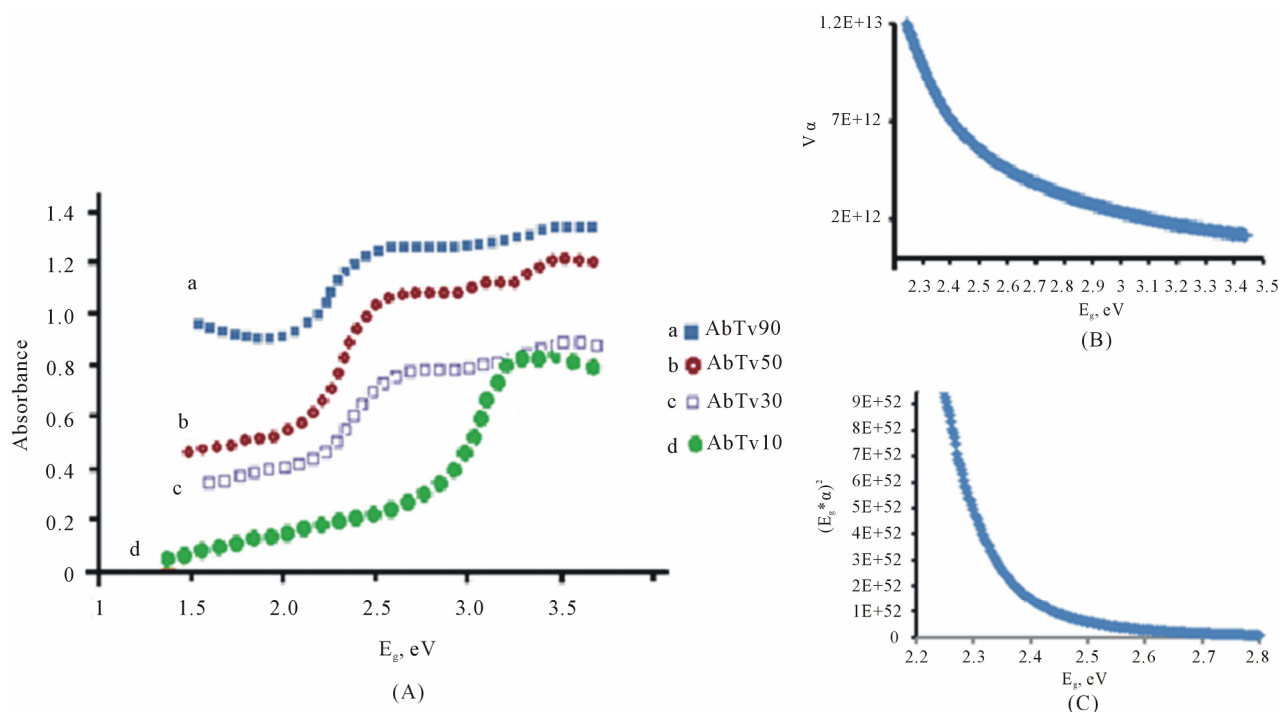
The plot of $\alpha^{1/2}$ vs E_g will lead to identification of indirect band transitions, while the plot of $(\alpha E_g)^2$ vs E_g will allow the determination of the direct transitions. These plots are known as Tauc plots. The results of these treatments are displayed in **Figures 3(B)** and **(C)** for 10% TiO₂/90% V₂O₅ mixture. The rest of the data listed in table 1 are results of the analysis of Tauc plots.

The data listed in **Table 1** indicates that increasing the percentage of V₂O₅ in the mixture clearly reduces the band gap to lesser values than that with pure TiO₂. Furthermore, both direct and indirect band gaps exist for these mixtures. However, the value of indirect band gap was in some cases greater than the direct band gap. Such unusual behavior can be attributed to the crystal growth structure discussed in the previous section. The fact that in all of the studies mixtures were active in photo reduction of $[\text{Fe}(\text{CN})_6]^{3-}$, indicates that the change in the value of the band gap resulted from shifting the valance band to less positive potential vs NHE. The data listed in **Table 1** also show that at 50% or greater percent of V₂O₅ in the mixture does not affect the value of the band gap.

Furthermore, TiO₂ doped with V₂O₅ possess an indirect band gap of $E_g \approx 2.8$ eV, this is greater than the direct band gap with a value of $E_g \approx 2.5$ eV, which is unexpected value of the studied mixture. This result suggests that TiO₂ has an indirect band gap transition when doped with V⁺⁵. It is known that the depletion layer width decreases with increasing distance of the energy level of the doping material from the conduction band.

Table 1. Band gap data for TiO₂/V₂O₅ mixtures.

V ₂ O ₅ % in TiO ₂ /V ₂ O ₅ mixtures	Band gap, eV	Direct band gap, eV	Indirect Band gap, eV
10	3.1	2.65	2.9
30	3.0	2.65	2.7
50	2.45	2.45	2.60
90	2.38	2.40	2.55

**Figure 3. (A) Steady state reflectance spectra for TiO₂/V₂O₅ mixtures; (B), (C) Tauc plots for indirect and direct band gap TiO₂/V₂O₅(50/50) mixture.**

The V₂O₅ oxides dopants energy levels are not located very far further from the conduction band of TiO₂. This increases the depletion layer width and consequently enhances charge transfer at the TiO₂/electrolyte interface.

3.3. Photolysis of Aqueous Doped Oxide Nano-Particles Colloidal Solutions

The photochemical behavior of these mixtures will be judged by its contribution to the photo-reduction current in total photo-electrochemical reduction current recorded during the photolysis process.

This can be explained using **Figure 4** which illustrates this process. Photolysis of [Fe(CN)₆]⁴⁻ according to Equation (2) in oxide-free solution, results in formation of [Fe(CN)₆]³⁻. Electrochemical reduction of [Fe(CN)₆]³⁻ generates the peak (a), in **Figure 4(A)**. In the presence of metal oxide mixtures, the recorded electrochemical reduction peak (b), is less in height than peak (a). This is

attributed to the fact that, in the presence of semiconductor p-type oxides, a portion of [Fe(CN)₆]⁴⁻ will be adsorbed on the surface of the oxide, which makes the recorded electrochemical reduction current of the working electrode is less than in the absence of the oxide particles or $I_{\text{homogeneous}} > I_{\text{heterogeneous}}$.

Where $I_{\text{homogeneous}} = I$ (recorded in the absence of oxide particles)

And $I_{\text{heterogeneous}} = I$ (recorded in the presence of oxide particles)

The photochemical reduction due to oxides = $I_{\text{homogeneous}} - I_{\text{heterogeneous}}$ ⁷

It is worth noticing that **Figure 4** shows that photolysis of homogenous solutions [Fe(CN)₆]⁴⁻ reaches a peak current with a very short plateau, while the photolysis of heterogeneous suspension of [Fe(CN)₆]⁴⁻ (in presence of metal oxides) reaches smaller peak height with a longer plateau. The longer period of reporting electrochemical

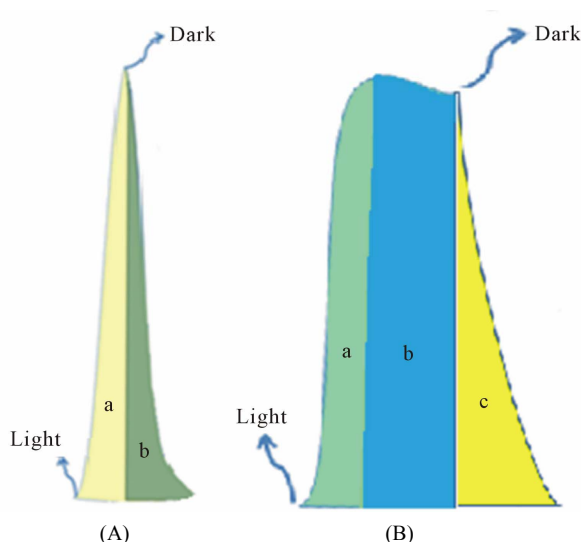


Figure 4. Illustration of dark and illumination current in case of: (A) In homogenous solution; (B) In heterogenous solution (Presence of the oxides).

reduction current in the heterogeneous suspension than in homogenous solutions can be attributed to the extra supply of $[\text{Fe}(\text{CN})_6]^{3-}$ (as photo oxidation products) that is desorbed from the surfaces of the nanoparticles of the oxides and reached the Pt working electrode in later time. Sections (b) in **Figure 4(A)** and section (c) in **Figure 4(B)**, represents electrochemical reduction current in darkness. We will refer to it from now on as “dark current”. In both homogenous and heterogeneous systems studied in this work, the electrochemical reduction current is supposed to drop to zero in the dark; however that is not the case as **Figure 5** illustrates. The reported electrochemical reduction current in darkness, in the case of a homogeneous solution, can be attributed to the radial diffusion of $[\text{Fe}(\text{CN})_6]^{3-}$ in the cylindrical zone of the Pt gauze electrode. The shape of the working electrode disrupts the continuity of the stirring effects, and makes the diffusion within the cylindrical shape a major factor for the reduction current. The dark current reported for heterogeneous systems (dashed traces in **Figure 5**) can be attributed to the desorption of $[\text{Fe}(\text{CN})_6]^{3-}$ from the surfaces of the oxide particles. The adsorption of $[\text{Fe}(\text{CN})_6]^{4-}$, and the desorption of its oxidized form $[\text{Fe}(\text{CN})_6]^{3-}$ on the surfaces of metal oxide nanoparticles is controlled by the metal oxide mixture composition.

3.4. Role of the Oxide Nanoparticles in Photolysis Process

When oxide nanoparticles are added to $[\text{Fe}(\text{CN})_6]^{4-}$ solutions, portion of them will be adsorbed on the surface of the particle. Such adsorption will retard reaction 2. This is because of adsorption, the interaction of $[\text{Fe}(\text{CN})_6]^{4-}$

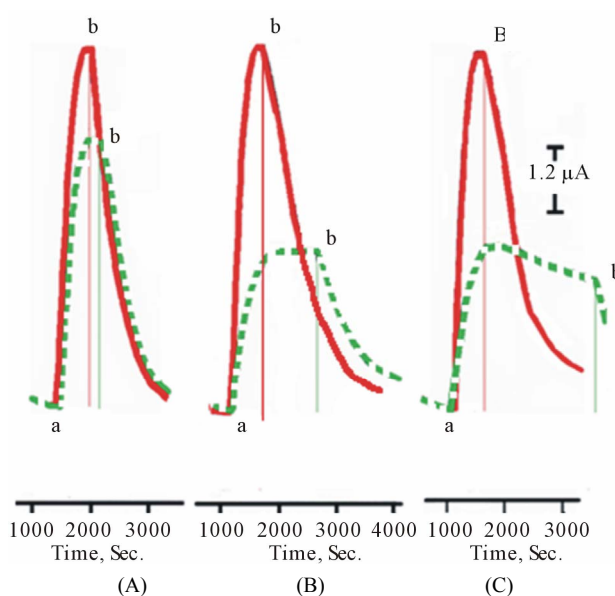


Figure 5. Photoelectrochemical response of working electrode during the photolysis of colloidal nano-particles of TiO₂ doped with V₂O₅ in 20 mM of K₄[Fe(CN)₆] in 0.2 M Phosphate buffer (pH = 6), (A) TiO₂doped with 10% V₂O₅; (B) TiO₂doped with 50% V₂O₅, and (C) V₂O₅ doped with 10% TiO₂; points a and b refers to illumination and dark respectively.

with the surface states created during the doping process took place. Upon illumination of the oxide particles, an (e/h) will be formed. The emitted electron will reduce H₃O⁺ ions, while $[\text{Fe}(\text{CN})_6]^{4-}$ acts as hole scavenger and is oxidized to $[\text{Fe}(\text{CN})_6]^{3-}$. Per each H₂ molecule is formed, two $[\text{Fe}(\text{CN})_6]^{4-}$ will be oxidized and still adsorbed on the surface of the oxides particle. As long as $[\text{Fe}(\text{CN})_6]^{4-}$ is oxidized on the particle surface and reduced in working electrode, the cyclic nature of this reaction will continue. The photo-interaction of the oxide particles with adsorbed $[\text{Fe}(\text{CN})_6]^{4-}/[\text{Fe}(\text{CN})_6]^{3-}$ is represented by section (b) in **Figure 4(B)**. This section possesses a plateau and the longer the plateau, the better the photo-chemical efficiency of the metal oxide semiconductor particles. This is because the length of the plateau reflects a steady state reversible oxidation reduction process of $[\text{Fe}(\text{CN})_6]^{4-}/[\text{Fe}(\text{CN})_6]^{3-}$.

3.5. Photolysis of Aqueous Colloidal TiO₂/V₂O₅ Mixtures

Photolysis of aqueous suspensions of TiO₂ mixed with 10%, 30%, and 50% V₂O₅ and V₂O₅ mixed with 10% TiO₂ took place as described in the experimental sections. The results are recorded in **Table 2** and **Figure 5**. **Table 2** indicates that the photo-reduction of $[\text{Fe}(\text{CN})_6]^{3-}$ to $[\text{Fe}(\text{CN})_6]^{4-}$ caused by the oxide mixture nanoparticle increased by increasing the percentage of V₂O₅ percent

Table 2. Steady state photo-current for studied metal oxides nano-particles at pH = 6 in 20 mM K₄[Fe(CN)₆] at -100 mV vs Ag/AgCl electrode.

Percentage of V ₂ O ₅ in TiO ₂	I, mA in [Fe(CN) ₆] ⁴⁻ , (electrochemical current)	I, mA in [Fe(CN) ₆] ⁴⁻ + Oxides, (electrochemical current)	I _{photo} , mA due to oxides Photocurrent	% I _{photo} due to Oxides only
10	5.76	4.42	1.34	23.6
30	5.39	3.39	2.00	37.1
50	5.85	3.07	2.78	47.5
90	5.65	3.22	2.43	43.0

age in the oxide mixture. Such results are consistent with the decrease of the band gap of TiO₂ with increasing V₂O₅ present (Table 1). Lowering the band gap increases the absorption in the visible region of the solar spectrum and consequently increases the photo-reduction by the p-type semiconductor. When TiO₂ becomes the dopant in V₂O₅ (10% TiO₂ with 90% V₂O₅) the photo-reduction drops back slightly to lower value than that of 50% V₂O₅.

3.6. Effect of V₂O₅

Two important observations that were reported in this work demonstrate the major effect of V₂O₅; 1) A more efficient photo-response was reported when nanoparticles of TiO₂ doped with V₂O₅ were suspended in buffered [Fe(CN)₆]⁴⁻; 2) The reproducible reactivity of these aqueous suspensions for a long time without deactivation which reflects their stability against photo corrosion. Our studies [4] indicated that TiO₂ doped with 5% V₂O₅ gives the greatest effect in phosphate buffer. Vanadium (V⁺⁵) facilitates the transfer of charge carriers at the interface because of alteration of the flat-band potential, and increases the absorption of incident light energy as a result of the increase in depletion layer width at the junction [21]. V⁺⁵ also supplied a high density of states that lower the band gap of TiO₂ and changed its band gap transition from direct to indirect transitions.

4. Conclusions

Increasing the percentage of V₂O₅ in TiO₂, cause noticeable changes in the growth and orientation of each oxide in their common crystal structure as evident from X-ray studies. Such changes create a diverse crystal structure leading to polymorphism solid. The random growth affected the nature and concentration of surface states. The fact that, the photocurrent of the TiO₂ doped with V₂O₅ was greater than that of TiO₂ can be attributed to 1) The high surface state density introduced by the diffusion of vanadium ions, and 2) Decreasing the rate of electron-hole recombination due to the change of the band transition mechanism from direct to indirect. The possibility of using these systems in a solar energy based photolysis

cell that would achieve the goal of a cyclic, and efficient process for hydrogen production is explored.

5. Acknowledgements

This work was supported by Indiana University Summer faculty fellowship program

REFERENCES

- [1] D. Martel, C. Nguyen, Hoan and J. Weiss, "Process for the Production of Hydrogen from an Aqueous Medium," France Patent No. 2940263, 2010.
- [2] V. M. Aroutiounian, V. M. Arakelyan and G. E. Shah-nazaryan, "Metal Oxide Photoelectrodes for Hydrogen Generation Using Solar Radiation-Driven Water Splitting," *Solar Energy*, Vol. 78, No. 5, 2005, pp. 581-592. [doi:10.1016/j.solener.2004.02.002](https://doi.org/10.1016/j.solener.2004.02.002)
- [3] M. Kaneko, H. Ueno, R. Saito, S. Yamaguchi, Y. Fujii and J. Nemoto, "UV Light-Activated Decomposition/Cleaning of Concentrated Biomass Wastes Involving also Solid Suspensions with Remarkably High Quantum Efficiency," *Applied Catalysis B: Environmental*, Vol. 91, No. 1-2, 2009, pp. 254-261. [doi:10.1016/j.apcatb.2009.05.033](https://doi.org/10.1016/j.apcatb.2009.05.033)
- [4] K. K. Kasem and M. Dahn, "Photodissociation of Water Using Colloidal Nanoparticles of Doped Titanium (IV) Oxide Semiconductors for Hydrogen Production," *Current Science*, Vol. 99, No. 8, 2010, pp. 1068-1073.
- [5] C. E. Jones and L. J. Carpenter, "Solar Photolysis of CH₂I₂, CH₂Cl, and CH₂IBr in Water, Saltwater, and Seawater," *Environmental Science and Technology*, Vol. 39, No. 16, 2005, pp. 6130-6137. [doi:10.1021/es050563g](https://doi.org/10.1021/es050563g)
- [6] V. M. Daskalaki, P. Panagiotopoulou and D. I. Kondarides, "Production of Peroxide Species in Pt/TiO₂ Suspensions under Conditions of Photocatalytic Water Splitting and Glycerol Photoreforming," *Chemical Engineering Journal*, Vol. 170, No. 2-3, 2011, pp. 433-439. [doi:10.1016/j.cej.2010.11.093](https://doi.org/10.1016/j.cej.2010.11.093)
- [7] K. K. Kasem, M. Dahn and N. Zia, "Photolysis of Aqueous Colloidal Zinc Oxide Nanoparticles for Hydrogen Production," *CACS Communications*, Vol. 4, No. 1, 2010, pp. 13-17.
- [8] A. Patsoura, D. I. Kondarides and X. E. Verykios, "Enhancement of Photoinduced Hydrogen Production from

- Irradiated Pt/TiO₂ Suspensions with Simultaneous Degradation of Azo-Dyes,” *Applied Catalysis B: Environmental*, Vol. 64, No. 3-4, 2006, pp. 171-179. doi:10.1016/j.apcatb.2005.11.015
- [9] K. Pechstedt, T. Whittle, J. Baumberg and T. Melvin, “Photoluminescence of Colloidal CdSe/ZnS Quantum Dots: The Critical Effect of Water Molecules,” *Journal of Physical Chemistry C*, Vol. 114, No. 28, 2010, pp. 12069-12077. doi:10.1021/jp100415k
- [10] M. Graetzel, “Nanocrystalline Electronic Junctions,” In: P. V. Kamat and D. Meisel, Eds., *Semiconductor Nano-clusters—Physical, Chemical and Catalytic Aspects*, Elsevier, Amsterdam, 1997, p. 353.
- [11] K. R. Goidas, M. Bohorques and P. V. Kamat, “Photo-physical and Photochemical Aspects of Coupled Semiconductors: Charge-Transfer Processes in Colloidal Cadmium Sulfide-Titania and Cadmium Sulfide-Silver(I) Iodide Systems,” *Journal of Physical Chemistry B*, Vol. 94, No. 16, 1990, pp. 6435-6440. doi:10.1021/j100379a051
- [12] R. Vogel, K. Pohl and H. Weller, “Sensitization of Highly Porous, Polycrystalline TiO₂ Electrodes by Quantum Sized CdS,” *Chemical Physics Letters*, Vol. 174, No. 3-4, 1990, pp. 241-246. doi:10.1016/0009-2614(90)85339-E
- [13] S. Kohtani, A. Kudo and T. Sakata, “Spectral Sanitization of TiO₂ Semiconductor Electrode by CdS Microcrystals, and Its Photoelectrochemical Properties,” *Chemical Physics Letters*, Vol. 206, No. 1-4, 1993, pp. 166-170. doi:10.1016/0009-2614(93)85535-V
- [14] R. Vogel, P. Hoyer and H. Weller, “Quantum-Sized PbS, CdS, Ag₂S, Sb₂S₃, and Bi₂S₃ Particles as Sensitizers for Various Nanoporous Wide-Bandgap Semiconductors,” *Journal of Physical Chemistry*, Vol. 98, No. 12, 1994, pp. 3183-3188. doi:10.1021/j100063a022
- [15] R. Plass, S. Pelet, J. Krueger, M. Gratzel and U. Bach, “Quantum Dot Sensitization of Organic—Inorganic Hybrid Solar Cells,” *Journal of Physical Chemistry B*, Vol. 106, No. 31, 2002, pp. 7578-7580. doi:10.1021/jp020453I
- [16] L. M. Peter, K. G. U. Wijayantha, D. J. Riley and J. P. Waggett, “Band-Edge Tuning in Self-Assembled Layers of Bi₂S₃ Nanoparticles Used to Photosensitize Nanocrystalline TiO₂,” *Journal of Physical Chemistry B*, Vol. 107, No. 33, 2003, pp. 8378-8381. doi:10.1021/jp030334I
- [17] S. Gordon, E. J. Hars, M. S. Matheson, J. Rahani and J. K. Thomas, “Reaction Constant of Hydrated Electrons,” *Journal of the American Chemical Society*, Vol. 85, No. 10, 1963, pp. 1375-1377. doi:10.1021/ja00893a002
- [18] A. Ookubo, E. Kanazaki and K. Ooi and Langmuir, “ESR, XRD, and DRS Studies of Paramagnetic Titanium(3+) Ions in a Colloidal Solid of Titanium Oxide Prepared by the Hydrolysis of Titanium Trichloride,” *Langmuir*, Vol. 6, No. 1, 1990, p. 206.
- [19] A. L. Patterson, “The Scherrer Formula for X-Ray Particle Size Determination,” *Physical Review Letters*, Vol. 56, No. 10, 1939, pp. 978-982. doi:10.1103/PhysRev.56.978
- [20] R. A. Van leeuwen, C.-J. Hung, D. R. Kammler and J. A. Switzer, “Optical and Electronic Transport Properties of Electrodeposited Thallium (III) Oxide Films,” *Journal of Physical Chemistry*, Vol. 99, No. 41, 1995, pp. 15247-15252. doi:10.1021/j100041a047
- [21] S. Kumari, C. Tripathi, A. P. Singh¹, D. Chauhan, R. Shrivastav, S. Dass and V. R. Satsangi, “Characterization of Zn-Doped Hematite Thin Films for Photoelectrochemical Splitting of Water,” *Current Science*, Vol. 91, No. 8, 2006, pp. 1062-1064.